

Numerical study on a post-processing method for Reissner-Mindlin plate finite elements

Jukka Aalto and Eero-Matti Salonen

Summary. The paper presents an element by element post-processing method for improving bending and twisting moments and shear forces, which can be used in connection with some simple Reissner-Mindlin plate elements. The method is restricted to straight sided triangular and quadrilateral elements, whose degrees of freedom are the deflections and rotations of the corner nodes. Experimental convergence studies for demonstrating the efficiency of the technique are given.

Key words: Reissner-Mindlin plates, finite elements, post-processing, stress-resultants

The plate elements

We consider in this paper triangular and quadrilateral elements (Figure 1) with three and four nodes, respectively. In the following we use the symbol n ($n = 3$ or $n = 4$) for the number of corner nodes of the element. In order to perform the derivations concisely, we consider a typical element side ij or a typical node j , which is connected to element sides ij and jk . After an equation corresponding to element side ij or a node j has been obtained, it can be applied for all the element sides or nodes using cyclic permutation 1,2,3 or 1,2,3,4 of the indices i, j , etc..

The length of the element side ij is

$$h_{ij} = \sqrt{(x_j - x_i)^2 + (y_j - y_i)^2} \quad (1)$$

and the cosine and sine of the direction angles of the element side are

$$c_{ij} = \cos \alpha_{ij} = \frac{x_j - x_i}{h_{ij}}, \quad s_{ij} = \sin \alpha_{ij} = \frac{y_j - y_i}{h_{ij}}. \quad (2)$$

The degrees of freedom of these original plate elements are the nodal deflections w_j and rotations¹ θ_{xj} and θ_{yj} $j = 1, \dots, n$ (see Figure 2).

¹ The term 'rotation' is used to denote the longer terms 'rotation of the normal' in the following.

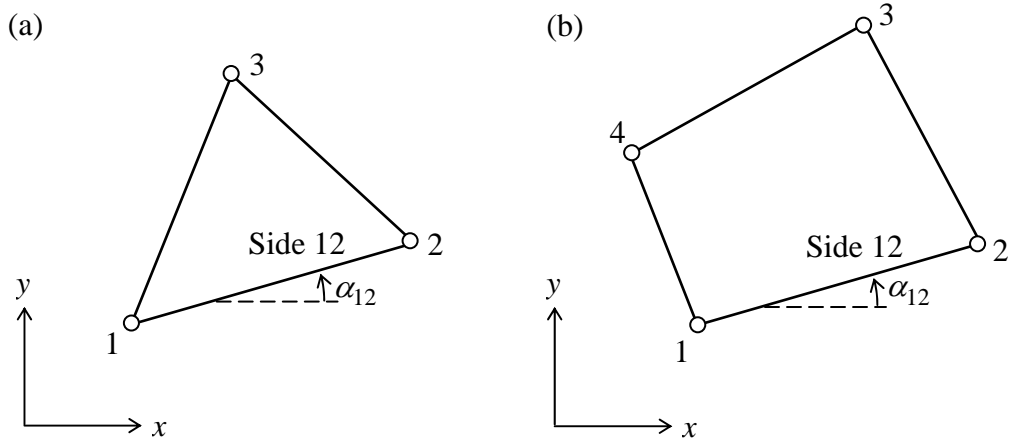


Figure 1: (a) A three node triangular and (b) a four node quadrilateral element.

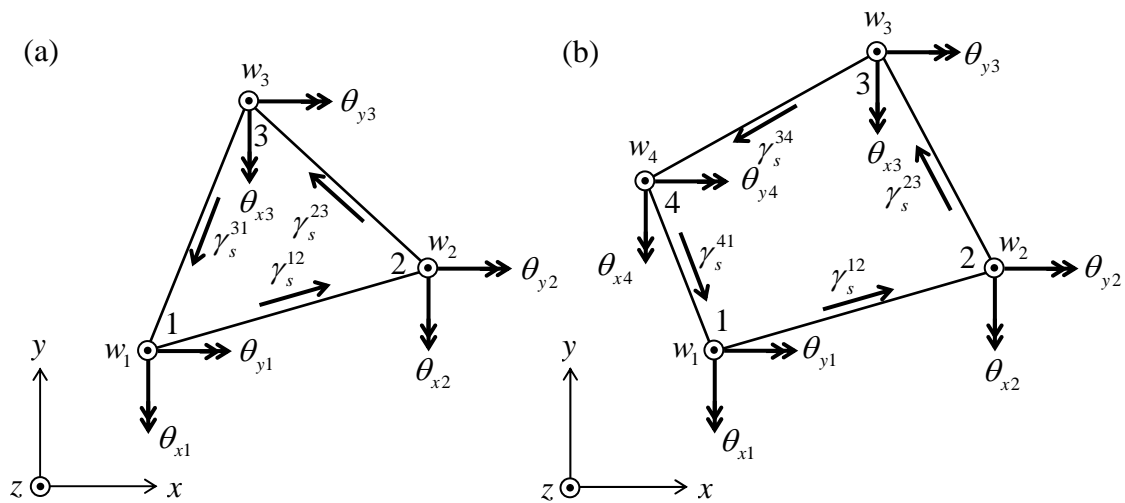


Figure 2: Nodal deflections and rotations and tangential shears of element sides in (a) triangular and (b) quadrilateral Reissner-Mindlin elements.

Nodal curvatures and shears

Assumptions

The purpose of the proposed post-processing technique is to construct improved nodal values for the curvatures and shears², which can then be used to obtain improved linear or bilinear approximations to these kinematic quantities within the element. With the

² The terms ‘curvatures’ and ‘shears’ are used to denote the longer term ‘curvatures and twist’ and ‘transverse shear strains’ in the following.

help of these the moments³ and shear forces are obtained straightforwardly based moment-curvature and shear force-shear relations. The starting points of improving the approximations of the curvatures is to (i) represent the deflection and shear along the element sides as a cubic polynomial and a constant, respectively, and (ii) to assume the rotation transverse the side to be linear along the element sides. The idea of approximating the curvatures and shears of this paper has already been applied in connection with simple Reissner-Mindlin plate elements of reference [1]. Therefore detailed derivation of results, which have already been presented in that reference, is not repeated here.

Nodal curvatures in terms of the nodal degrees of freedom of the element and shear parameters

The deflection $\tilde{w}(s)$ along the element side ij is assumed to be cubic and using Hermitean shape functions of form

$$\tilde{w}^{ij} = H_1 w_i + H_2 (\theta_s^{ij})_i + H_3 w_j + H_4 (\theta_s^{ij})_j + (H_2 + H_4) \gamma_s^{ij} \quad (3)$$

Here w_i and w_j are the deflections at nodes i and j , respectively, $(\theta_s^{ij})_i$ and $(\theta_s^{ij})_j$ are the rotations along side ij at nodes i and j , respectively, and parameter γ_s^{ij} (see Figure 2) is the tangential component of shear on side ij , which is assumed to be constant. With the help of the expression $\theta_s = w_{,s} - \gamma_s$ the rotation along the element side can also be expressed in terms of the same parameters and it can further be differentiated to get its derivative $\theta_{s,s}$ with respect to the side coordinate s . Thus it is possible to get such derivatives on sides ij and jk and further their values $(\theta_{s,s}^{ij})_j$ and $(\theta_{s,s}^{jk})_j$ at node j . Using the linearity assumption of the transverse rotation θ_n along element sides, it is possible to express its derivatives $(\theta_{n,s}^{ij})_j$ and $(\theta_{n,s}^{jk})_j$ at node j in terms of the nodal rotations. Thereafter it is possible to express the Cartesian derivatives $(\theta_{x,x})_j$, $(\theta_{x,y})_j$, $(\theta_{y,x})_j$ and $(\theta_{y,y})_j$ of the rotation components at node j in terms of the obtained derivatives $(\theta_{s,s}^{ij})_j$, $(\theta_{s,s}^{jk})_j$, $(\theta_{n,s}^{ij})_j$ and $(\theta_{n,s}^{jk})_j$. Finally the curvatures at node j can be evaluated from $\kappa_x = -\theta_{x,x}$, $\kappa_y = -\theta_{y,y}$ and $2\kappa_{xy} = -\theta_{x,y} - \theta_{y,x}$. With the help of the described sequence of operations the nodal curvatures κ_{xj} , κ_{yj} and $2\kappa_{xyj}$ can be expressed linearly in terms of the nodal deflections, nodal rotations and the tangential shears of the element sides. The resulting relationships can be written as

$$\mathbf{k} = \mathbf{Aa} + \mathbf{Bb}, \quad (4)$$

³ The term ‘moments’ is used to denote the longer term ‘bending moments and twisting moment’ in the following.

where

$$\begin{aligned}
\mathbf{k}_{3n \times 1} &= \left[\kappa_{x1} \quad \kappa_{y1} \quad 2\kappa_{xy1} \quad \cdots \quad \kappa_{xn} \quad \kappa_{yn} \quad 2\kappa_{xyn} \right]^T, \\
\mathbf{a}_{3n \times 1} &= \left[w_1 \quad \theta_{x1} \quad \theta_{y1} \quad \cdots \quad w_n \quad \theta_{xn} \quad \theta_{yn} \right]^T, \\
\mathbf{b}_{n \times 1} &= \left[\gamma_s^{12} \quad \cdots \quad \gamma_s^{n1} \right]^T.
\end{aligned} \tag{5}$$

are column vectors of the nodal curvatures, nodal deflections and rotations and tangential shears of the element sides, respectively. The improved curvature approximation (4) is thus defined by the known nodal parameters \mathbf{a} of the applied plate element and n ($n = 3$ triangle, $n = 4$ quadrilateral) additional unknown parameters \mathbf{b} , which are called here shear parameters. These parameters are not necessarily available and it will be shown in the following, how they can be determined. The elements of matrices \mathbf{A} and \mathbf{B} are listed in appendix A. Detailed derivation of these results has been presented in appendix A of reference [1].

Nodal shears in terms of the shear parameters

It is possible to express the nodal Cartesian shear components γ_{xj} and γ_{yj} at node j linearly in terms of the tangential shears γ_s^{ij} and γ_s^{jk} . The derivation of this result is based on the assumption, that the tangential shears are constants along the element sides. The result corresponding to each node can be written as

$$\mathbf{g} = \mathbf{C}\mathbf{b}, \tag{6}$$

where

$$\mathbf{g}_{2n \times 1} = \left[\gamma_{x1} \quad \gamma_{y1} \quad \cdots \quad \gamma_{xn} \quad \gamma_{yn} \right]^T. \tag{7}$$

The elements of the corresponding matrix \mathbf{C} are given in appendix A. Detailed derivation of this result has been presented in appendix B of reference [1]. This derivation is based on the shear approximation first presented in references [2] and [3].

Nodal moments and shear forces

The plate moment curvature relation is of form

$$\mathbf{M} = \mathbf{D}_\kappa \mathbf{\kappa}, \tag{8}$$

where \mathbf{D}_κ is the moment curvature matrix and $\boldsymbol{\kappa}$ the vector of the curvatures κ_x , κ_y and twice the twist κ_{xy} . In the special case of an isotropic plate, which we use in the numerical examples, we present it in the form

$$\mathbf{D}_\kappa = D_b \begin{bmatrix} 1 & \nu & 0 \\ \nu & 1 & 0 \\ 0 & 0 & (1-\nu)/2 \end{bmatrix}, \quad (9)$$

where D_b is the bending stiffness and ν Poisson's ratio. For a homogeneous plate and a thin face sandwich plate the bending stiffnesses are

$$D_b = \frac{Eh^3}{12(1-\nu^2)} \quad \text{and} \quad D_b = \frac{E_f d^2 t}{2}, \quad (10)$$

respectively. E is the modulus of elasticity and h the thickness of the homogeneous plate and E_f modulus of elasticity, d distance and t thickness of the faces of the sandwich plate. For a homogeneous plate both in equations (9) and (10a) ν is the Poisson's ratio of the plate and for a sandwich plate in equation (9) ν is the Poisson's ratio of the faces.

Applying relations (8) at each node, the nodal moments can be expressed in terms of the nodal curvatures $\boldsymbol{\kappa}$ by

$$\mathcal{M} = \mathcal{D}_\kappa \boldsymbol{\kappa}, \quad (11)$$

where

$$\mathcal{M}_{3n \times 1} = \begin{bmatrix} M_{x1} & M_{y1} & M_{xy1} & \cdots & M_{xn} & M_{yn} & M_{xyn} \end{bmatrix}^T, \quad \mathcal{D}_{3n \times 3n} = \begin{bmatrix} \mathbf{D}_\kappa & \mathbf{0} & \mathbf{0} \\ \mathbf{0} & \mathbf{D}_\kappa & \mathbf{0} \\ \mathbf{0} & \mathbf{0} & \mathbf{D}_\kappa \end{bmatrix}. \quad (12)$$

The plate shear force shear relation is of form

$$\mathbf{Q} = \mathbf{D}_\gamma \boldsymbol{\gamma}, \quad (13)$$

where \mathbf{D}_γ is the shear force shear matrix and $\boldsymbol{\gamma}$ the vector of the shears γ_x and γ_y . In the special case of an isotropic plate we present it in the form

$$\mathbf{D}_\gamma = D_s \begin{bmatrix} 1 & 0 \\ 0 & 1 \end{bmatrix}, \quad (14)$$

where D_s is shear stiffness. For a homogeneous plate and a thin face sandwich plate the shear stiffnesses are

$$D_s = kGh \quad \text{and} \quad D_c = G_c d, \quad (15)$$

respectively. Here $k = 5/6$ is the shear correction factor and G the shear modulus of the homogeneous plate and G_c the shear modulus of the core of the sandwich plate.

Applying relations (13) at each node, the nodal shear forces can be expressed in terms of the nodal shears \mathbf{g} by

$$\mathcal{Q} = \mathcal{D}_\gamma \mathbf{g}, \quad (16)$$

where

$$\underset{2n \times 1}{\mathcal{Q}} = \left[Q_{x1} \quad Q_{y1} \quad \cdots \quad Q_{xn} \quad Q_{yn} \right]^T, \quad \underset{2n \times 2n}{\mathcal{D}_\gamma} = \begin{bmatrix} \mathbf{D}_\gamma & \mathbf{0} \\ \mathbf{0} & \mathbf{D}_\gamma \end{bmatrix}. \quad (17)$$

Determining the shear parameters

Least squares equations

In the following the shear parameters \mathbf{b} are determined by demanding first the plate equilibrium equations

$$Q_x = M_{x,x} + M_{xy,y}, \quad Q_y = M_{xy,x} + M_{y,y} \quad (18)$$

to hold in least squares sense at the nodal points of the element. The least squares condition is

$$s \equiv (\mathcal{Q} - \bar{\mathcal{Q}})^T (\mathcal{Q} - \bar{\mathcal{Q}}) = \min, \quad (19)$$

where \mathcal{Q} is the vector of nodal shear forces of the element and $\bar{\mathcal{Q}}$ is the corresponding vector calculated using equations (18), whose elements corresponding to node j are

$$\bar{Q}_{xj} = (M_{x,x})_j + (M_{xy,y})_j, \quad \bar{Q}_{yj} = (M_{xy,x})_j + (M_{y,y})_j. \quad (20)$$

With the help of equations (16) the least squares condition (19) gets the form

$$s \equiv (\mathcal{D}_\gamma \mathbf{Cb} - \bar{\mathcal{Q}})^T (\mathcal{D}_\gamma \mathbf{Cb} - \bar{\mathcal{Q}}) = \min. \quad (21)$$

Based on this condition the set of equations for the shear parameters \mathbf{b} becomes

$$\mathbf{C}^T \mathcal{D}_\gamma \mathcal{D}_\gamma \mathbf{Cb} = \mathbf{C}^T \mathcal{D}_\gamma \bar{\mathcal{Q}}. \quad (22)$$

Expressing the nodal shear forces \bar{Q} in terms of the nodal moments \mathcal{M}

Let us determine the derivatives of the bending moment M_x at node j , if its nodal values at nodes i , j and k are known. Its derivatives along sides ij and jk at node j can be written as

$$\begin{aligned}(M_{x,sij})_j &= c_{ij}(M_{x,x})_j + s_{ij}(M_{x,y})_j, \\ (M_{x,sjk})_j &= c_{jk}(M_{x,x})_j + s_{jk}(M_{x,y})_j.\end{aligned}\quad (23)$$

By inverting these relations we get for the corresponding Cartesian derivatives

$$\begin{aligned}(M_{x,x})_j &= \frac{1}{d_j} [s_{jk}(M_{x,sij})_j - s_{ij}(M_{x,sjk})_j], \\ (M_{x,y})_j &= \frac{1}{d_j} [-c_{jk}(M_{x,sij})_j + c_{ij}(M_{x,sjk})_j],\end{aligned}\quad (24)$$

where

$$d_j = c_{ij}s_{jk} - s_{ij}c_{jk}.\quad (25)$$

Because the distribution of the bending moment M_x along the element sides is assumed to be linear, its derivatives on these sides ij and jk are constants and of form

$$M_{x,sij} = \frac{M_{xj} - M_{xi}}{h_{ij}}, \quad M_{x,sjk} = \frac{M_{xk} - M_{xj}}{h_{jk}}.\quad (26)$$

These results apply also at node j and thus using equations (24) we can write for the Cartesian derivatives of the bending moment M_x at node j the result

$$\begin{aligned}(M_{x,x})_j &= -\frac{s_{jk}}{d_j h_{ij}} M_{xi} + \frac{1}{d_j} \left(\frac{s_{jk}}{h_{ij}} + \frac{s_{ij}}{h_{jk}} \right) M_{xj} - \frac{s_{ij}}{d_j h_{jk}} M_{xk}, \\ (M_{x,y})_j &= +\frac{c_{jk}}{d_j h_{ij}} M_{xi} - \frac{1}{d_j} \left(\frac{c_{jk}}{h_{ij}} + \frac{c_{ij}}{h_{jk}} \right) M_{xj} + \frac{c_{ij}}{d_j h_{jk}} M_{xk}.\end{aligned}\quad (27)$$

Similar results are obtained for the Cartesian derivatives of the bending moment M_y and the twisting moment M_{xy} at node j . Equations (20) now give for the shear forces \bar{Q}_x and \bar{Q}_y at node j

$$\begin{aligned}
\bar{Q}_{xj} &= -\frac{s_{jk}}{d_j h_{ij}} M_{xi} + \frac{c_{jk}}{d_j h_{ij}} M_{xyi} + \frac{1}{d_j} \left(\frac{s_{jk}}{h_{ij}} + \frac{s_{ij}}{h_{jk}} \right) M_{xj} \\
&\quad - \frac{1}{d_j} \left(\frac{c_{jk}}{h_{ij}} + \frac{c_{ij}}{h_{jk}} \right) M_{xyj} - \frac{s_{ij}}{d_j h_{jk}} M_{xk} + \frac{c_{ij}}{d_j h_{jk}} M_{xyk}, \\
\bar{Q}_{yj} &= -\frac{s_{jk}}{d_j h_{ij}} M_{xyi} + \frac{c_{jk}}{d_j h_{ij}} M_{yji} + \frac{1}{d_j} \left(\frac{s_{jk}}{h_{ij}} + \frac{s_{ij}}{h_{jk}} \right) M_{xyj} \\
&\quad - \frac{1}{d_j} \left(\frac{c_{jk}}{h_{ij}} + \frac{c_{ij}}{h_{jk}} \right) M_{yj} - \frac{s_{ij}}{d_j h_{jk}} M_{xyk} + \frac{c_{ij}}{d_j h_{jk}} M_{yjk}.
\end{aligned} \tag{28}$$

These results corresponding to each node can be expressed in matrix form as

$$\bar{\mathcal{Q}} = \mathbf{E}\mathcal{M}. \tag{29}$$

The elements of the corresponding matrix \mathbf{E} are given in appendix A.

Solving the shear parameters

Combining equations (4), (11), (22) and (29) gives the equation

$$\mathbf{G}\mathbf{b} = \mathbf{h}, \tag{30}$$

where

$$\mathbf{G} = \mathbf{C}^T \mathcal{D}_\gamma \mathcal{D}_\gamma \mathbf{C} - \mathbf{C}^T \mathcal{D}_\gamma \mathbf{E} \mathcal{D}_\kappa \mathbf{B} \tag{31}$$

and

$$\mathbf{h} = \mathbf{C}^T \mathcal{D}_\gamma \mathbf{E} \mathcal{D}_\kappa \mathbf{A}\mathbf{a}. \tag{32}$$

Equation (30) is the final set of equations for solving the shear parameters \mathbf{b} . It contains n (3 or 4) simultaneous equations.

Calculating the nodal moments and shear forces

After the shear parameters \mathbf{b} of the element are known, the element nodal curvatures \mathbf{k} and shears \mathbf{g} can be calculated using equations (4) and (6). With the help of these the element nodal moments \mathcal{M} and shear forces \mathcal{Q} can be calculated using equations (11) and (16).

Example problem

In order to study numerically the behavior of the proposed post-processing technique a simply supported square plate of Figure 3 is used as an example problem. In support case “hard” all the edges of the plate have “hard” simple supports and in support case “mixed” two opposite edges have “hard” and “soft” simple supports, respectively.

The example plate is loaded by sinusoidal load

$$q(x, y) = q_0 \sin\left(\pi \frac{x}{a}\right) \sin\left(\pi \frac{y}{a}\right). \quad (33)$$

Analytical solutions of a square Reissner-Mindlin plate under this load in both support cases considered are available and are used for comparison in the numerical examples given.

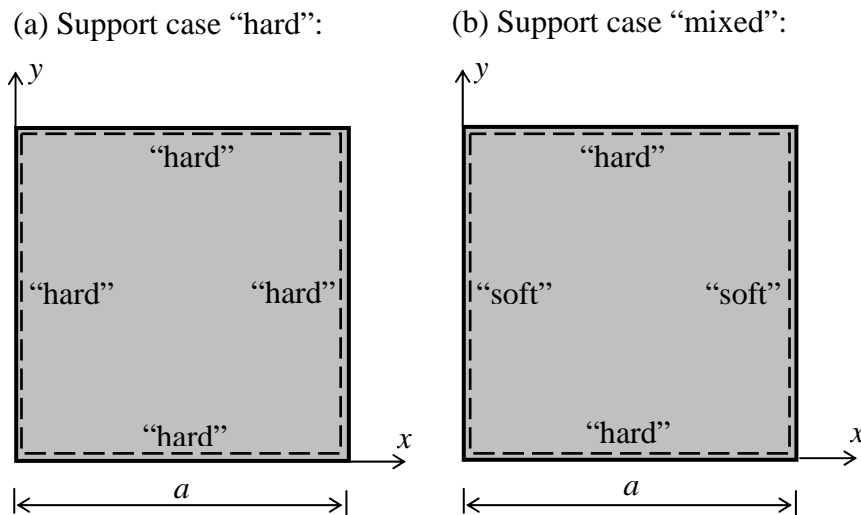


Figure 3: Simply supported square plate: (a) support case “hard” and (b) support case “mixed”

Typical cases of a homogenous plate and a sandwich plate are considered by using two values $\varepsilon = 0,01$ and $\varepsilon = 10$ for the dimensionless ratio

$$\varepsilon = \frac{D_b}{D_s a^2} \quad (34)$$

of the bending and shear stiffness D_b and D_s . In order to find out the effect of distortion of the finite element grid to the results in addition to uniform grids (Figures 4 (a) and 5 (a)) also slightly distorted (Figures 4 (b) and 5 (b)) grids of both triangular and quadrilateral elements were used. The distortion of the grid was obtained by moving the coordinates of the internal nodes randomly within a tolerance of $0,2h$.

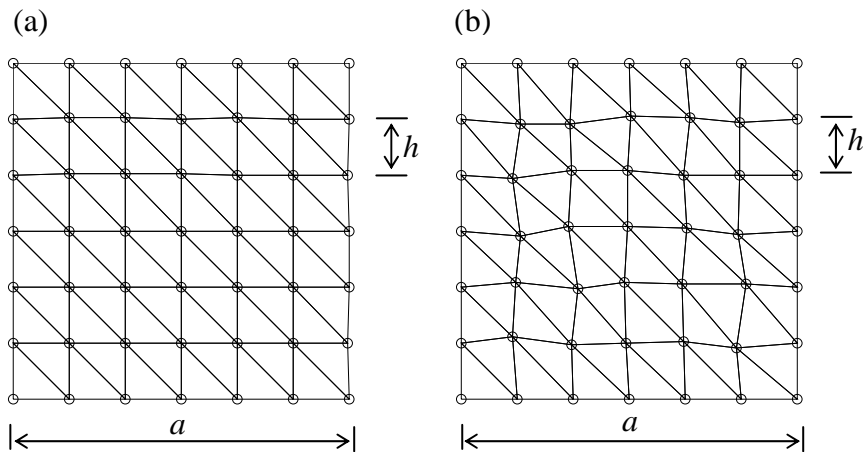


Figure 4: Typical grids ($n_{el} = 6$) of triangular elements: (a) uniform (b) distorted

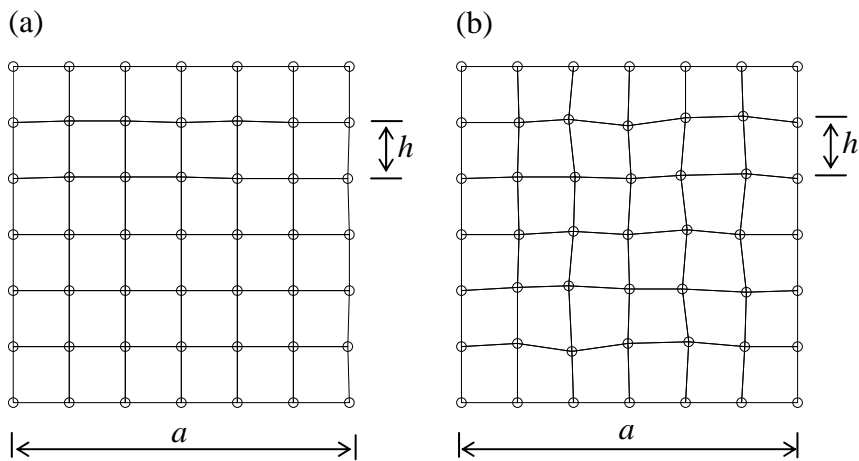


Figure 5: Typical grid ($n_{el} = 6$) of quadrilateral elements: (a) uniform (b) distorted

The behavior of the post-processing technique is studied both in ideal conditions, where the nodal parameters \mathbf{a}^e are taken from the analytical solution of the problem, and in practical conditions, where the nodal parameters \mathbf{a}^e are results of finite element analysis using simple Reissner-Mindlin plate elements. The elements used in this context are C^0 -continuous linear triangle with one point reduced integration and C^0 -continuous bilinear quadrilateral with selective reduced integration with 2×2 and 1×1 Gauss quadratures for the bending and shear parts of the stiffness matrix, respectively.

Special attention here is focused to the element nodal values of the moments and shear forces. In addition to the post-processed element nodal values of these quantities also the “consistent” nodal values obtained using the C^0 -continuous plate elements used are calculated. Because the shear force and moment approximations of the C^0 -continuous triangle are constants within the element, these values as such are taken as “consistent” element nodal values at each element node. Typically in connection with the selectively integrated C^0 -continuous quadrilateral the representative values of the moments and shear forces are at the four and one integration points, respectively. The corresponding “consistent” nodal values are thus obtained here by extrapolating these

values from the integration points to the element nodes using bilinear and constant interpolation, respectively.

In order to get a global measure of the accuracy of the obtained nodal moments and shear forces at the element nodes, relative error measures

$$\begin{aligned}\eta_M &= \sqrt{\frac{\sum_e (\mathcal{M}_{\text{appr}}^e - \mathcal{M}_{\text{exact}}^e)^T (\mathcal{M}_{\text{appr}}^e - \mathcal{M}_{\text{exact}}^e)}{\sum_e \mathcal{M}_{\text{exact}}^e T \mathcal{M}_{\text{exact}}^e}} 100\%, \\ \eta_Q &= \sqrt{\frac{\sum_e (\mathcal{Q}_{\text{appr}}^e - \mathcal{Q}_{\text{exact}}^e)^T (\mathcal{Q}_{\text{appr}}^e - \mathcal{Q}_{\text{exact}}^e)}{\sum_e \mathcal{Q}_{\text{exact}}^e T \mathcal{Q}_{\text{exact}}^e}} 100\%,\end{aligned}\tag{35}$$

are used here. In these expressions the summation is performed over the elements of the grid.

Results of numerical study of the example problem are described briefly in the following. A typical homogeneous plate and a typical sandwich plate with stiffness ratios $\varepsilon = 10$ and $\varepsilon = 0,01$, respectively, are considered. Analysis with both “hard” and “mixed” support conditions and regular and irregular grids, was performed. A careful comparison of post processed nodal shear forces and moments with the corresponding consistent ones is also made.

Numerical results with triangular elements

Numerical test results with triangular elements are here arranged as follows: Plots of dimensionless shear forces $Q_x/(q_0 a)$ and bending moments $M_x/(q_0 a^2)$ are shown in Figures 6 to 9. Experimental convergence plots of the error measures η_Q and η_M of the nodal shear forces and nodal moments, as a function of elements per side n_{el} , are shown in Figures B.1 to B.4 of appendix B. Results with distorted grids are only shown here, because the corresponding results with uniform grids were very similar.

In the “hard” support case, when the nodal parameters are taken from the analytical solution, the post-processed shear force and bending moment distributions seem to be good (Figures 6 and 7) and mostly better than the consistent ones. Also the convergence plots (Figure B.1) indicate, that both the nodal shear forces and moments converge. The distribution of the bending moment has clearly improved, but the shear forces seem to remain element by element constants. In sandwich plate case ($\varepsilon = 10$), the consistent and post-processed shear forces seem to coincide, but in homogeneous plate case ($\varepsilon = 0,01$), the post-processed shear forces are clearly better. Also, if the nodal parameters are calculated using finite element analysis with C^0 – continuous triangles and one point integration, the results remain very similar (Figure B.2).

In the “mixed” support case, when the nodal parameters are taken either from the analytical solution or from finite element results, the post processed shear forces behave much like in the “hard” support case (Figures 8a and 9a). There is, however, a dramatic

change in the behavior of the post-processed moments. Severe oscillations appear in the bending moment distributions (Figures 8b and 9b) and nodal moments do not converge at all (Figures B.3 and B.4).

Numerical results with quadrilateral elements

Numerical test results with quadrilateral elements are arranged as follows: Plots of dimensionless shear forces $Q_x/(q_0a)$ and bending moments $M_x/(q_0a^2)$ are shown in Figures 10 to 13. Experimental convergence plots of the error measures η_Q and η_M are shown in Figures B.5 to B.8 of appendix B. Results with distorted grids are only shown here.

In the “hard” support case, when the nodal parameters are either taken from the analytical solution or calculated using finite element analysis with C^0 – continuous quadrilaterals and selective integration, both the post-processed shear force and bending moment distributions are clearly better than the consistent ones (Figures 10 and 11). Also the convergence plots (Figures B.5 and B.6) indicate, that both the nodal shear forces and moments converge.

In the “mixed” support case the post-processed shear force and bending moment distributions are, by inspection, clearly better than the consistent ones (Figures 12 and 13). Convergence plots (Figures B.7b and B8.b) reveal, however, that results for the nodal moments in connection homogeneous plate case ($\varepsilon = 0,01$) are not, better than the consistent ones. Convergence plots (Figures B.7 and B.8) indicate, that both the nodal shear forces and moments converge. This is a remarkable difference compared to the triangular element.

A note on the shear approximation

The shear parameters γ_s^{12} , γ_s^{23} ... and γ_s^{n1} or elements of vector \mathbf{b} , are not independent, but related by a constraint equation

$$h^{12}\gamma_s^{12} + h^{23}\gamma_s^{22} + \dots h^{n1}\gamma_s^{n1} = 0, \quad (36)$$

which is based on compatibility of the shear deformation. This is shown in appendix C. Thus in connection with triangular and quadrilateral elements the shear approximation is presented using two and three independent parameters, respectively.

In a triangular element this is equivalent to the fact that the post-processed approximations of the Cartesian shear components γ_x and γ_y are constants within an element. This is shown in appendix D. If the shear force shear matrix \mathbf{D}_γ is constant within an element, also the post processed shear forces Q_x and Q_y will be element by element constants. This was actually observed in the numerical results with triangular elements.

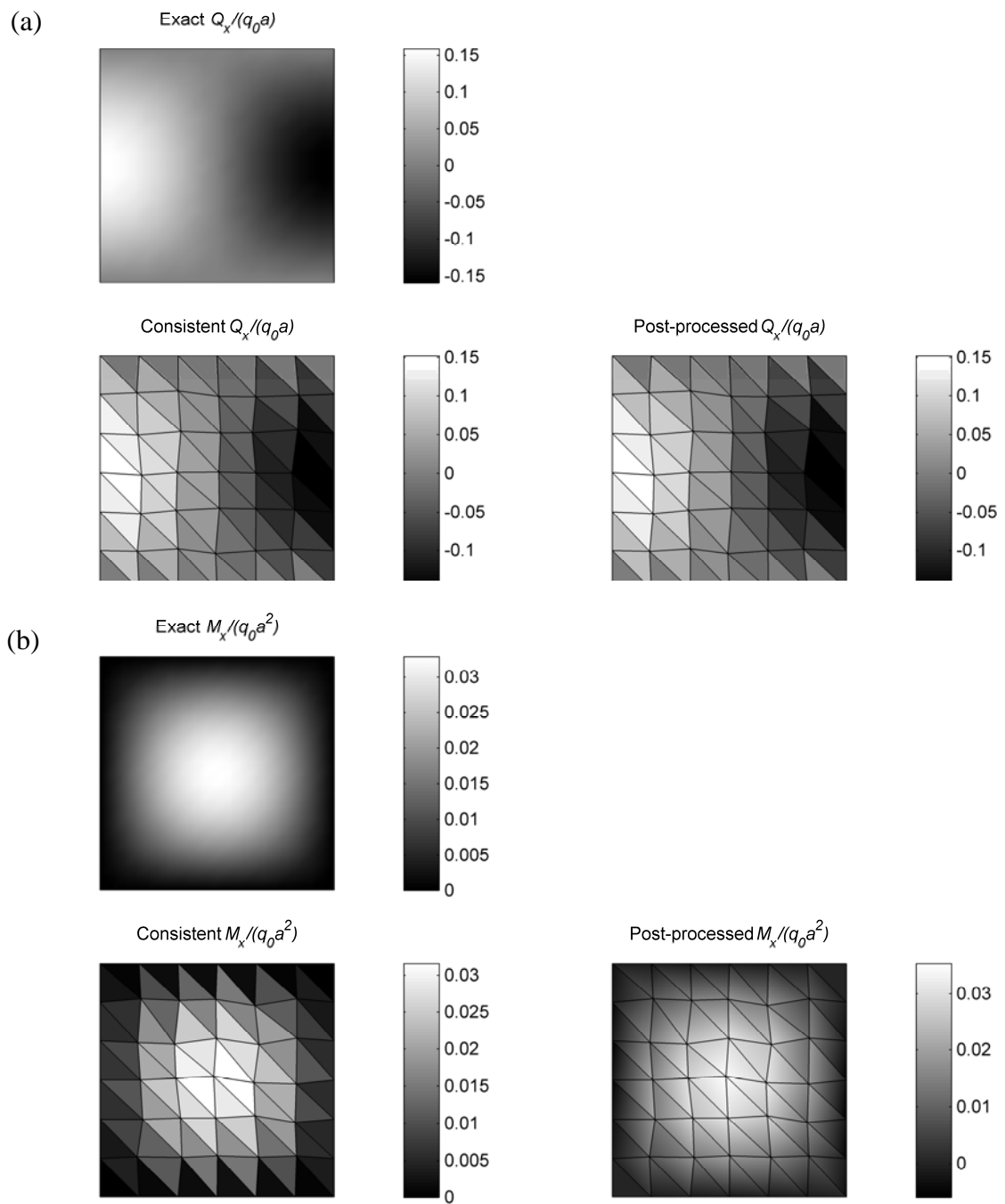


Figure 6: Triangular elements, “hard” supports, nodal parameters from the analytical solution, $\varepsilon = 10$

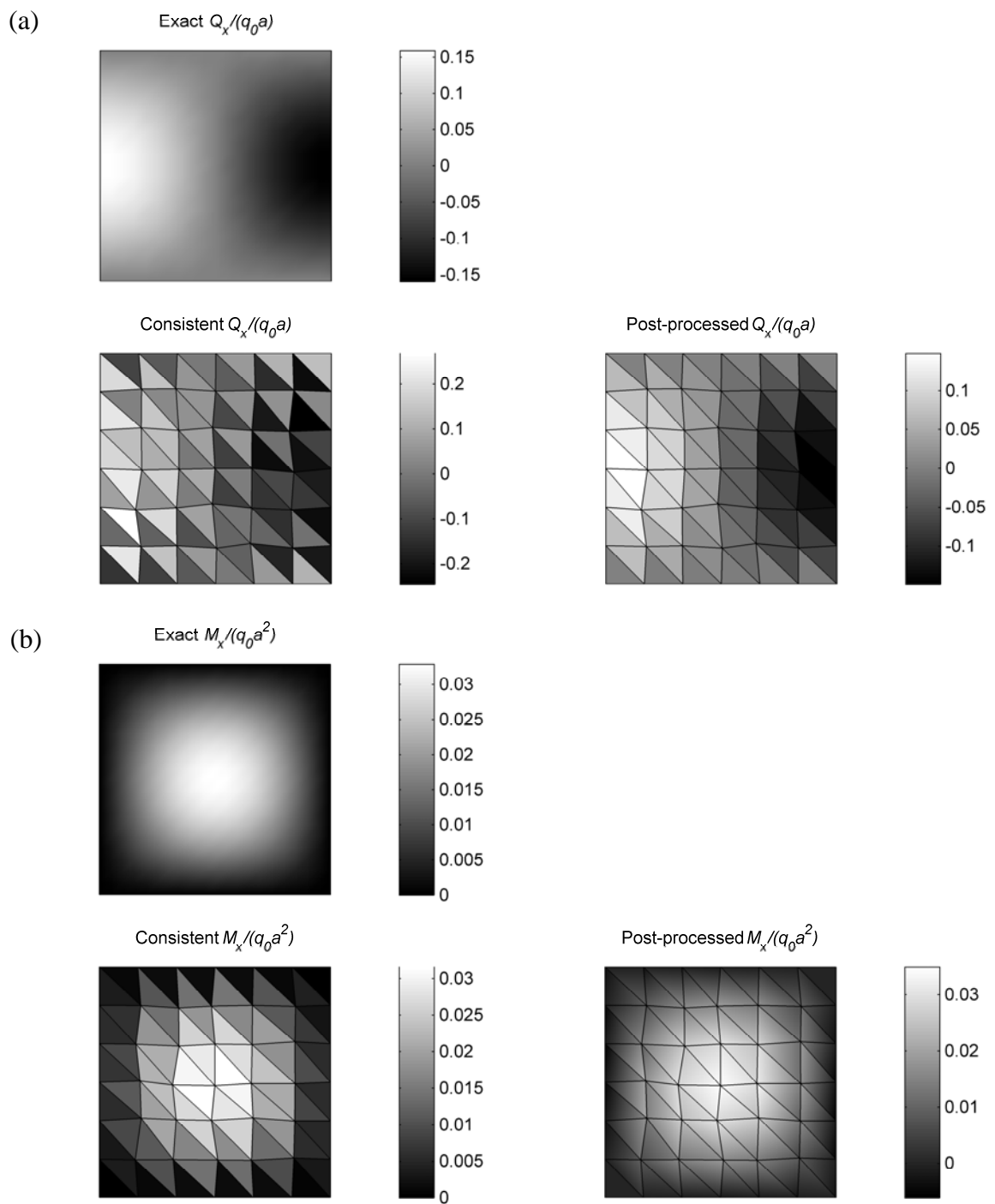


Figure 7: Triangular elements, “hard” supports, nodal parameters from the analytical solution, $\varepsilon = 0,01$

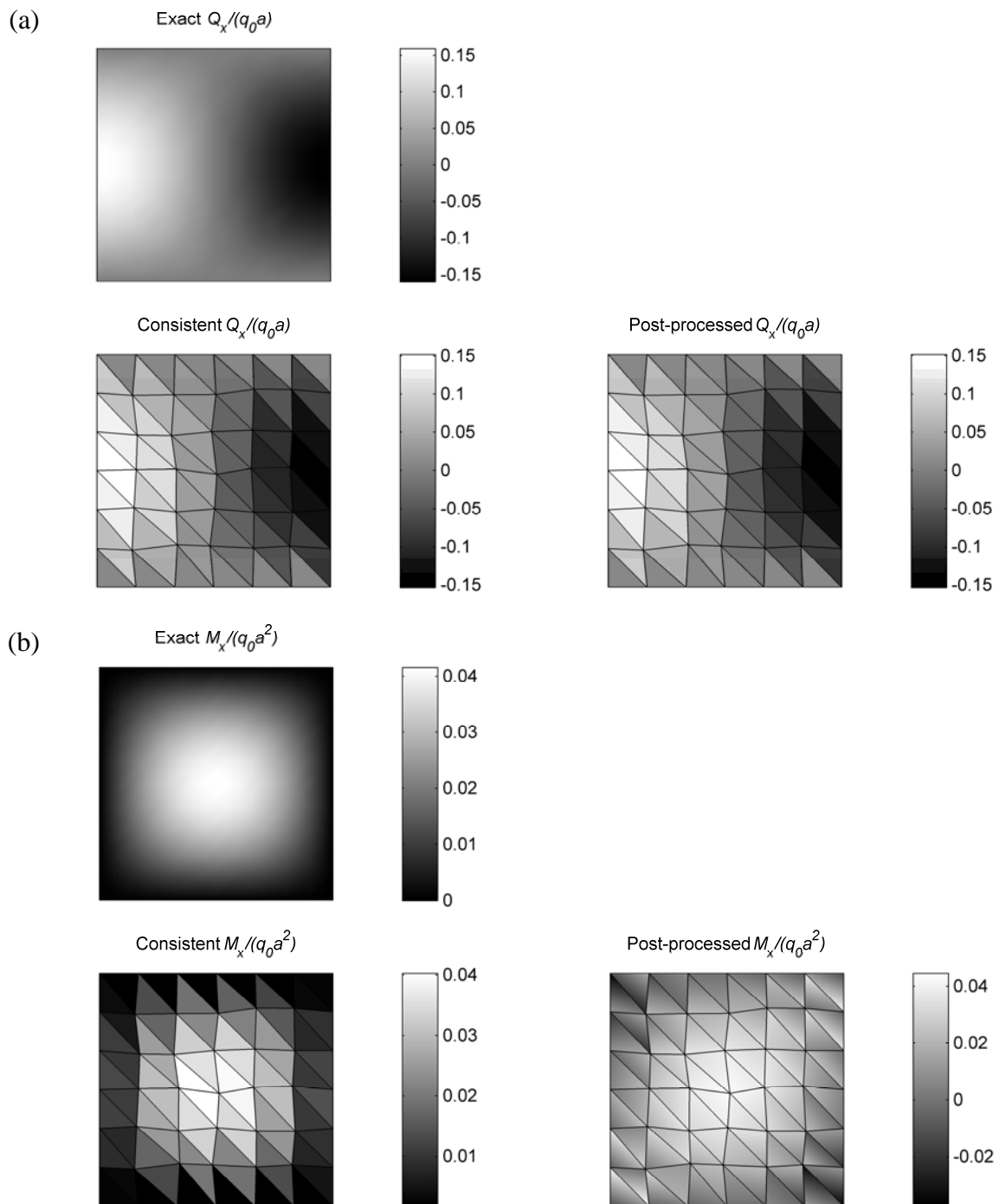


Figure 8: Triangular elements, “mixed” supports, nodal parameters from the analytical solution, $\varepsilon = 10$

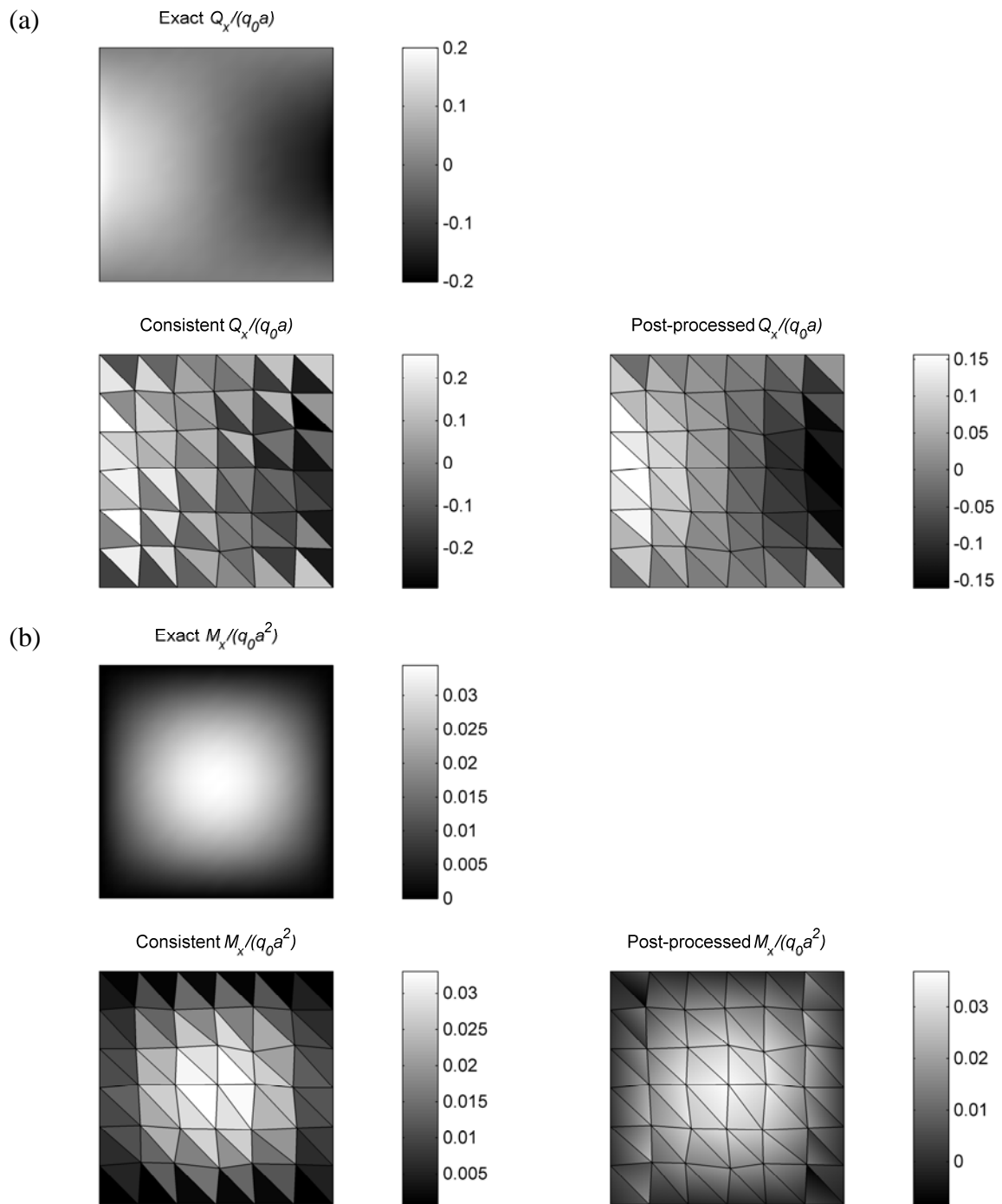


Figure 9: Triangular elements, “mixed” supports, nodal parameters from the analytical solution, $\varepsilon = 0,01$

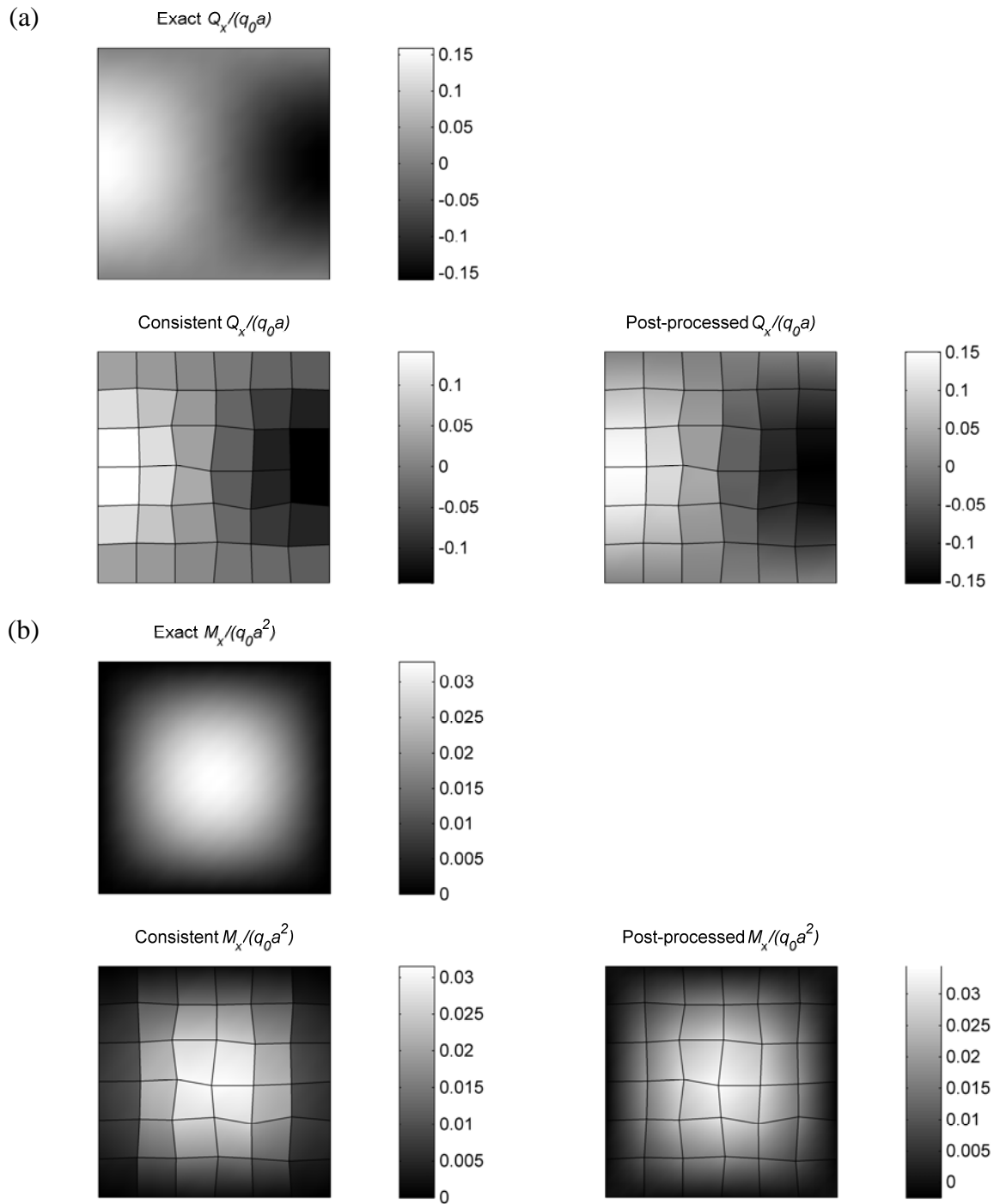


Figure10: Quadrilateral elements, “hard” supports, nodal parameters from the analytical solution, $\varepsilon = 10$

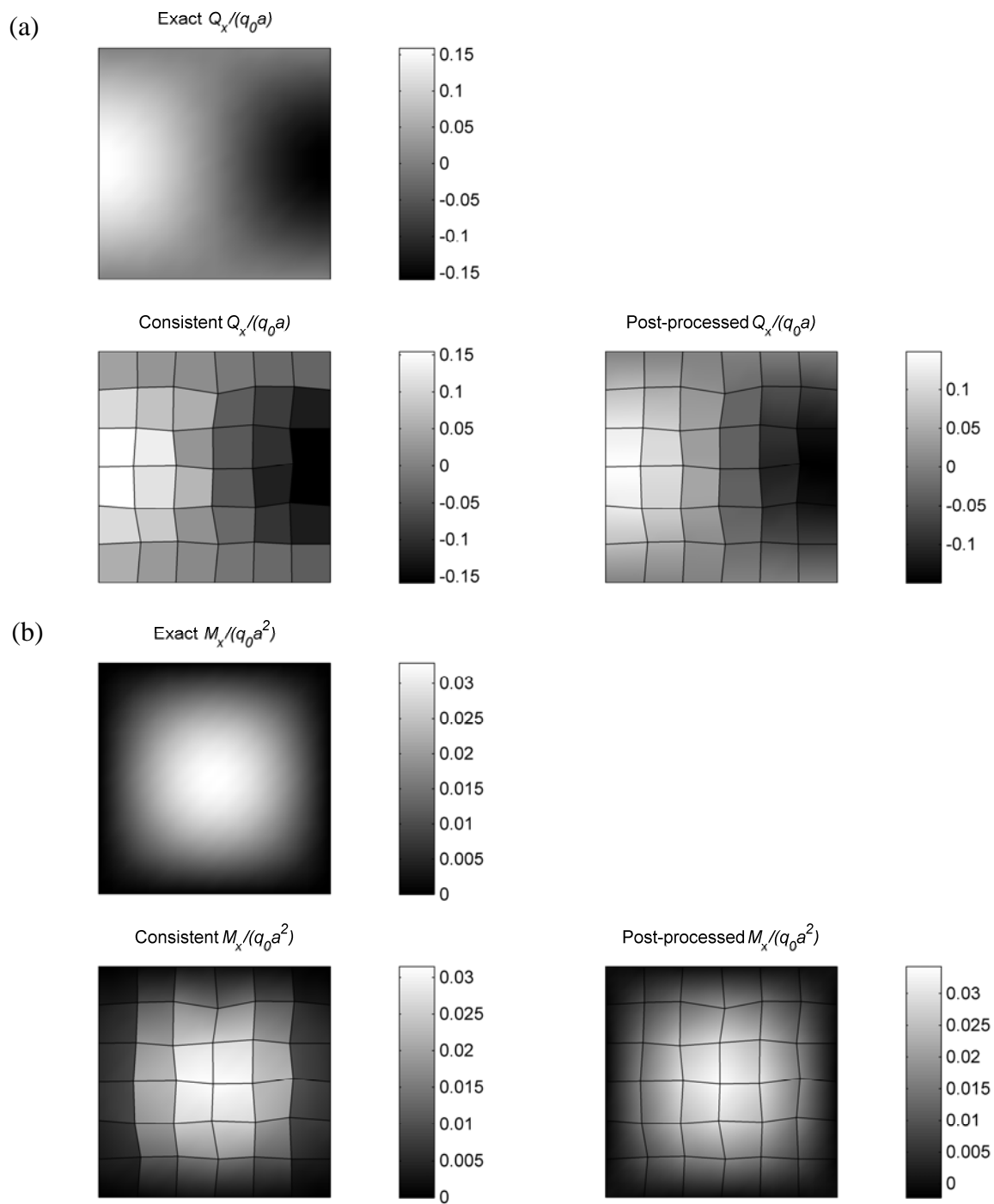


Figure 11: Quadrilateral elements, “hard” supports, nodal parameters from the analytical solution, $\varepsilon = 0,01$

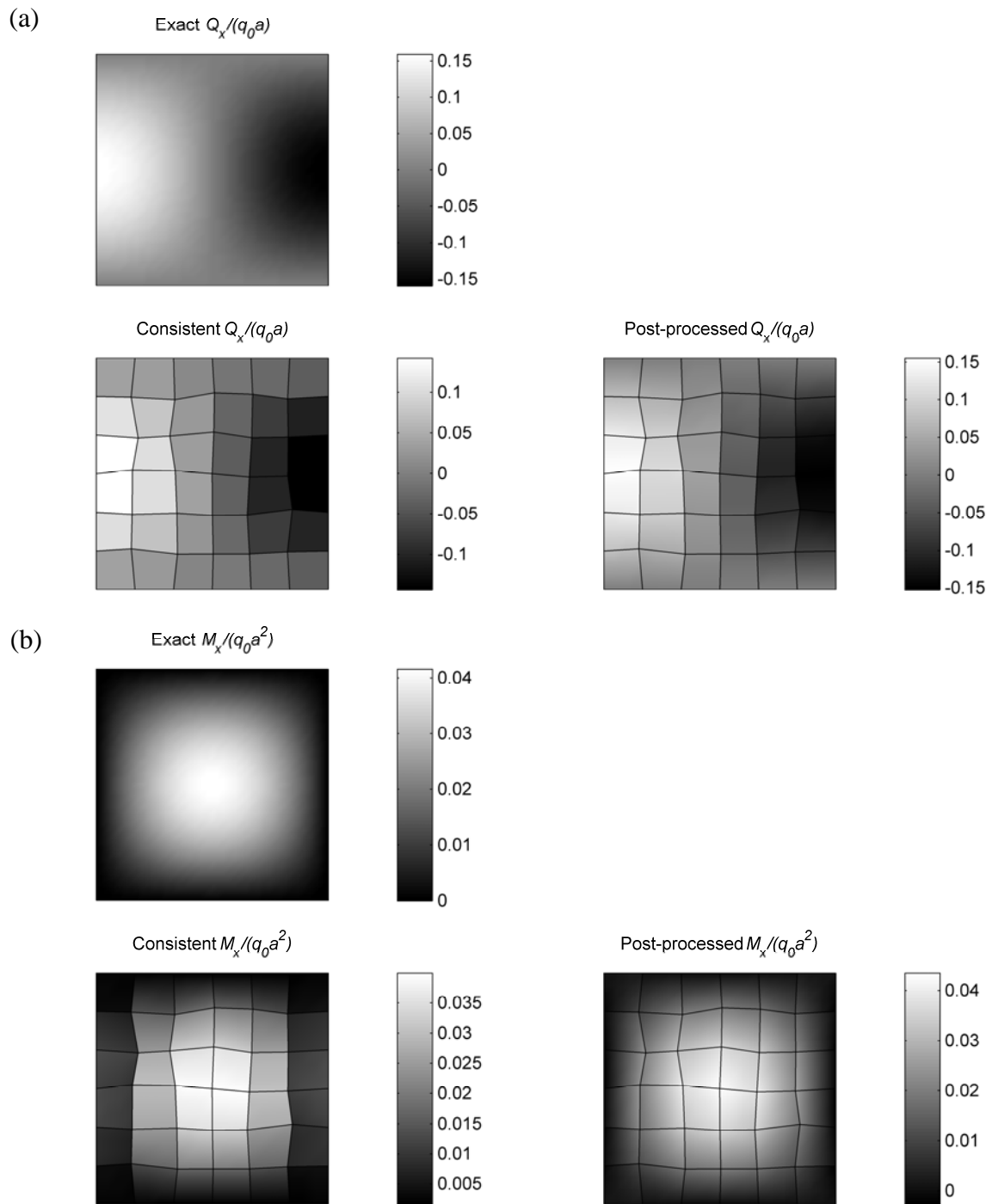


Figure 12: Quadrilateral elements, “mixed” supports, nodal parameters from the analytical solution, $\varepsilon = 10$

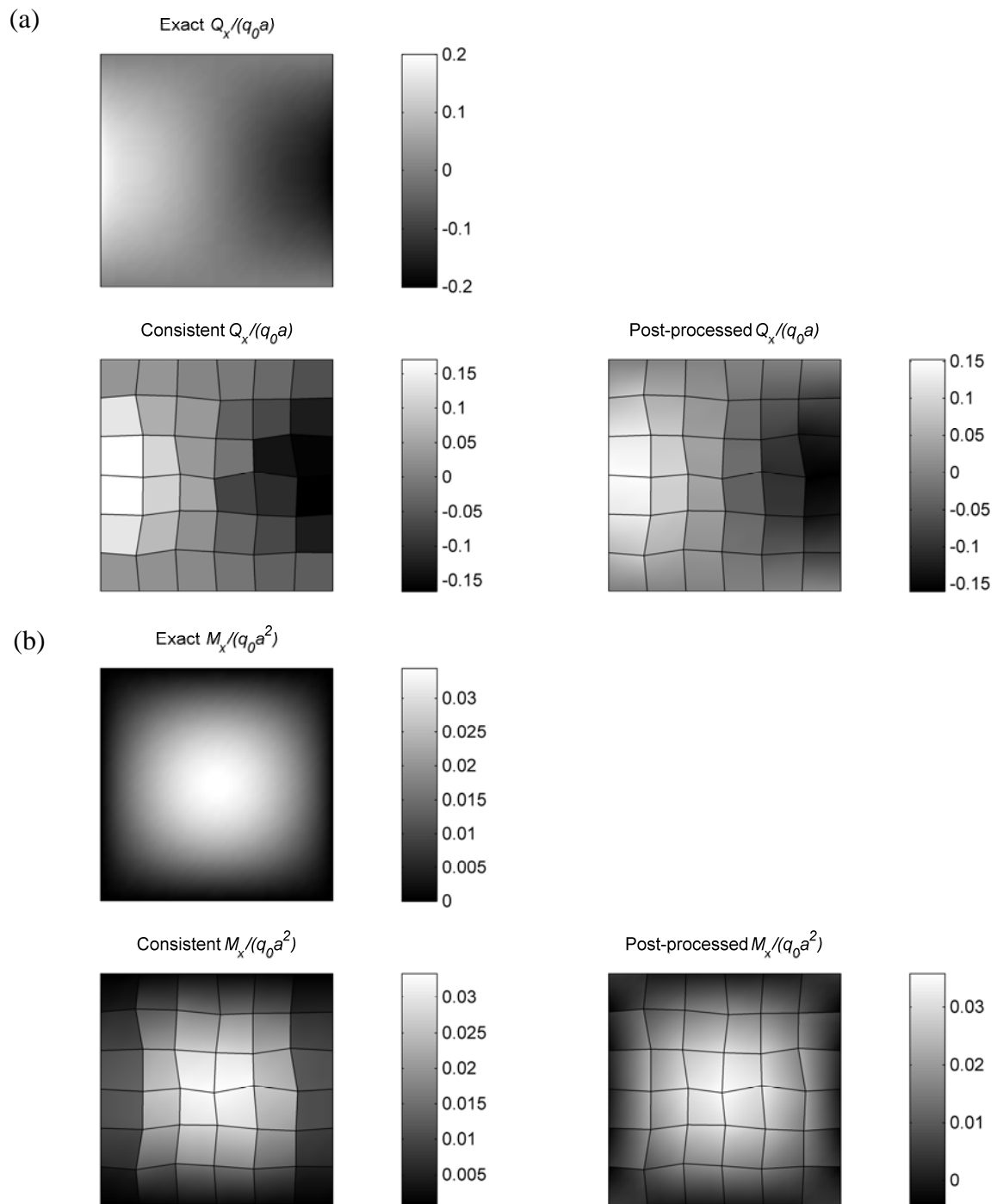


Figure 13: Quadrilateral elements, “mixed” supports, nodal parameters from the analytical solution, $\varepsilon = 0,01$

Conclusions

The given numerical results show, that the presented post-processing method works. In connection with triangular elements and “hard” supports both the post processed shear forces and bending moments converged, but in connection with “mixed” supports the post processed bending moments did not converge. These results indicate, that with triangular elements the method cannot handle the typical boundary layer of a Reissner-Mindlin plate solution properly. Therefore the presented post-processing method is not recommended to be used with three node triangular plate elements.

In connection with quadrilateral elements the post-processed shear forces and bending moments converged both in the “hard” and “mixed” support case. The post-processed shear forces and bending moments seemed to be smoother and converged mainly better than the consistent ones. Therefore the presented post-processing method can be used as one alternative in improving the shear force and bending moment results obtained using four node quadrilateral Reissner-Mindlin plate elements.

References

- [1] J. Aalto, On deriving of some simple plate elements, *Journal of Structural Mechanics*, 40(4), 55-79, 2007.
- [2] T.J.R. Hughes and R.L. Taylor, The linear triangular bending element, in *Proceedings of The Mathematics of Finite Elements and Applications IV MAFELAP 1981*, (Ed. J. R. Whiteman), Academic Press, London, 127-142, 1982.
- [3] T.J.R. Hughes and T.E. Tezduyar, Finite elements based upon Mindlin plate theory with particular reference to four node bilinear isoparametric element, *A.S.M.E Journal of Applied Mechanics*, 48, 587-596, 1981.

Jukka Aalto, Eero-Matti Salonen
Aalto University
Department of Structural Engineering and Building Technology
PO Box 12100, FIN-00076 Aalto, Finland
jukka.aalto@tkk.fi, eero-matti.salonen@tkk.fi

Appendix A: Elements of matrices **A**, **B**, **C** and **E**

The elements of matrix **A** can be obtained using equations

$$\begin{aligned}
A_{3j-2,3i-2} &= -\frac{6c_{ij}s_{jk}}{d_j h_{ij}^2}, \quad A_{3j-2,3i-1} = -\frac{s_{jk}}{d_j h_{ij}}(2c_{ij}^2 - s_{ij}^2), \quad A_{3j-2,3i} = -\frac{3s_{ij}s_{jk}c_{ij}}{d_j h_{ij}}, \\
A_{3j-2,3j-2} &= +\frac{6}{d_j} \left(\frac{c_{ij}s_{jk}}{h_{ij}^2} - \frac{s_{ij}c_{jk}}{h_{ij}^2} \right), \\
A_{3j-2,3j-1} &= -\frac{1}{d_j} \left[\frac{s_{jk}}{h_{ij}}(4c_{ij}^2 + s_{ij}^2) + \frac{s_{ij}}{h_{jk}}(4c_{jk}^2 + s_{jk}^2) \right], \\
A_{3j-2,3j} &= -\frac{3s_{ij}s_{jk}}{d_j} \left(\frac{c_{ij}}{h_{ij}} + \frac{c_{jk}}{h_{jk}} \right), \\
A_{3j-2,3k-2} &= +\frac{6s_{ij}c_{jk}}{d_j h_{jk}^2}, \quad A_{3j-2,3k-1} = -\frac{s_{ij}}{d_j h_{jk}}(2c_{jk}^2 - s_{jk}^2), \quad A_{3j-2,3k} = -\frac{3s_{ij}s_{jk}c_{jk}}{d_j h_{jk}}, \\
A_{3j-1,3i-2} &= +\frac{6s_{ij}c_{jk}}{d_j h_{ij}^2}, \quad A_{3j-1,3i-1} = +\frac{3s_{ij}c_{jk}c_{ij}}{d_j h_{ij}}, \quad A_{3j-1,3i} = +\frac{c_{jk}}{d_j h_{ij}}(2s_{ij}^2 - c_{ij}^2), \\
A_{3j-1,3j-2} &= -\frac{6}{d_j} \left(\frac{s_{ij}c_{jk}}{h_{ij}^2} - \frac{c_{ij}s_{jk}}{h_{jk}^2} \right), \quad A_{3j-1,3j-1} = +\frac{3c_{jk}c_{ij}}{d_j} \left(\frac{s_{ij}}{h_{ij}} + \frac{s_{jk}}{h_{ik}} \right), \\
A_{3j-1,3j} &= +\frac{1}{d_j} \left[\frac{c_{jk}}{h_{ij}}(4s_{ij}^2 + c_{ij}^2) + \frac{c_{ij}}{h_{jk}}(4s_{jk}^2 + c_{jk}^2) \right], \\
A_{3j-1,3k-2} &= -\frac{6c_{ij}s_{jk}}{d_j h_{jk}^2}, \quad A_{3j-1,3k-1} = +\frac{3c_{ij}s_{jk}c_{jk}}{d_j h_{jk}}, \quad A_{3j-1,3k} = +\frac{c_{ij}}{d_j h_{jk}}(2s_{jk}^2 - c_{jk}^2), \\
A_{3j,3i-2} &= +\frac{6}{d_j h_{ij}^2} (c_{ij}c_{jk} - s_{ij}s_{jk}), \quad A_{3j,3i-1} = +\frac{1}{d_j h_{ij}} [c_{jk}(2c_{ij}^2 - s_{ij}^2) - 3s_{ij}s_{jk}c_{ij}], \\
A_{3j,3i} &= -\frac{1}{d_j h_{ij}} [s_{jk}(2s_{ij}^2 - c_{ij}^2) - 3c_{ij}c_{jk}s_{ij}], \\
A_{3j,3j-2} &= +\frac{6(s_{12}s_{jk} - c_{12}c_{jk})}{d_j} \left(\frac{1}{h_{12}^2} - \frac{1}{h_{jk}^2} \right), \\
A_{3j,3j-1} &= +\frac{1}{d_j} \left[\frac{c_{jk}}{h_{ij}}(4c_{ij}^2 + s_{ij}^2) + \frac{c_{ij}}{h_{jk}}(4c_{jk}^2 + s_{jk}^2) - 3s_{ij}s_{jk} \left(\frac{c_{ij}}{h_{ij}} + \frac{c_{jk}}{h_{jk}} \right) \right], \\
A_{3j,3j} &= -\frac{1}{d_j} \left[\frac{s_{jk}}{h_{ij}}(4s_{ij}^2 + c_{ij}^2) + \frac{s_{ij}}{h_{jk}}(4s_{jk}^2 + c_{jk}^2) - 3c_{ij}c_{jk} \left(\frac{s_{ij}}{h_{ij}} + \frac{s_{jk}}{h_{jk}} \right) \right],
\end{aligned} \tag{A.1}$$

$$A_{3j,3k-2} = -\frac{6}{d_j h_{jk}^2} (c_{ij} c_{jk} - s_{ij} s_{jk}), \quad A_{3j,3k-1} = +\frac{1}{d_j h_{jk}} [c_{ij} (2c_{jk}^2 - s_{jk}^2) - 3s_{ij} s_{jk} c_{jk}],$$

$$A_{3j,3k} = -\frac{1}{d_j h_{jk}} [s_{ij} (2s_{jk}^2 - c_{jk}^2) - 3c_{ij} c_{jk} s_{jk}]$$

and cyclic permutation. The elements of matrix **B** can be obtained using equations

$$B_{3j-2,i} = -\frac{6c_{ij}s_{jk}}{d_j h_{ij}}, \quad B_{3j-2,j} = -\frac{6s_{ij}c_{jk}}{d_j h_{jk}},$$

$$B_{3j-1,i} = +\frac{6s_{ij}c_{jk}}{d_j h_{ij}}, \quad B_{3j-1,j} = +\frac{6c_{ij}s_{jk}}{d_j h_{jk}}, \quad (\text{A.2})$$

$$B_{3j,i} = -\frac{6(s_{ij}s_{jk} - c_{ij}c_{jk})}{d_j h_{ij}}, \quad B_{3i,j} = -\frac{6(s_{ij}s_{jk} - c_{ij}c_{jk})}{d_j h_{jk}}.$$

and cyclic permutation. The nonzero element of matrix **C** are obtained using equations

$$C_{2j-1,i} = \frac{s_{jk}}{d_j}, \quad C_{2j-1,j} = -\frac{s_{ij}}{d_j}, \quad C_{2j,i} = -\frac{c_{jk}}{d_j}, \quad C_{2j,j} = \frac{c_{ij}}{d_j} \quad (\text{A.3})$$

and cyclic permutation. The nonzero elements of matrix **E** are obtained using equations

$$E_{2j-1,3i-2} = -\frac{s_{jk}}{d_j h_{ij}}, \quad E_{2j-1,3i} = \frac{c_{jk}}{d_j h_{ij}},$$

$$E_{2j-1,3j-2} = \frac{1}{d_j} \left(\frac{s_{jk}}{h_{ij}} + \frac{s_{ij}}{h_{jk}} \right), \quad E_{2j-1,3j} = -\frac{1}{d_j} \left(\frac{c_{jk}}{h_{ij}} + \frac{c_{ij}}{h_{jk}} \right),$$

$$E_{2j-1,3k-2} = -\frac{s_{ij}}{d_j h_{jk}}, \quad E_{2j-1,3k} = \frac{c_{ij}}{d_j h_{jk}}, \quad (\text{A.4})$$

$$E_{2j,3i-1} = \frac{c_{jk}}{d_j h_{ij}}, \quad E_{2j,3i} = -\frac{s_{jk}}{d_j h_{ij}},$$

$$E_{2j,3j-1} = -\frac{1}{d_j} \left(\frac{c_{jk}}{h_{ij}} + \frac{c_{ij}}{h_{jk}} \right), \quad E_{2j,3j} = \frac{1}{d_j} \left(\frac{s_{jk}}{h_{ij}} + \frac{s_{ij}}{h_{jk}} \right),$$

$$E_{2j,3k-1} = \frac{c_{ij}}{d_j h_{jk}}, \quad E_{2j,3k} = -\frac{s_{ij}}{d_j h_{jk}}$$

and cyclic permutation. In all these equations $d_j = c_{ij}s_{jk} - s_{ij}c_{jk}$.

Appendix B: Experimental convergence plots of the error measures η_Q and η_M of the nodal shear forces and moments. Comparison of consistent and post-processed results.

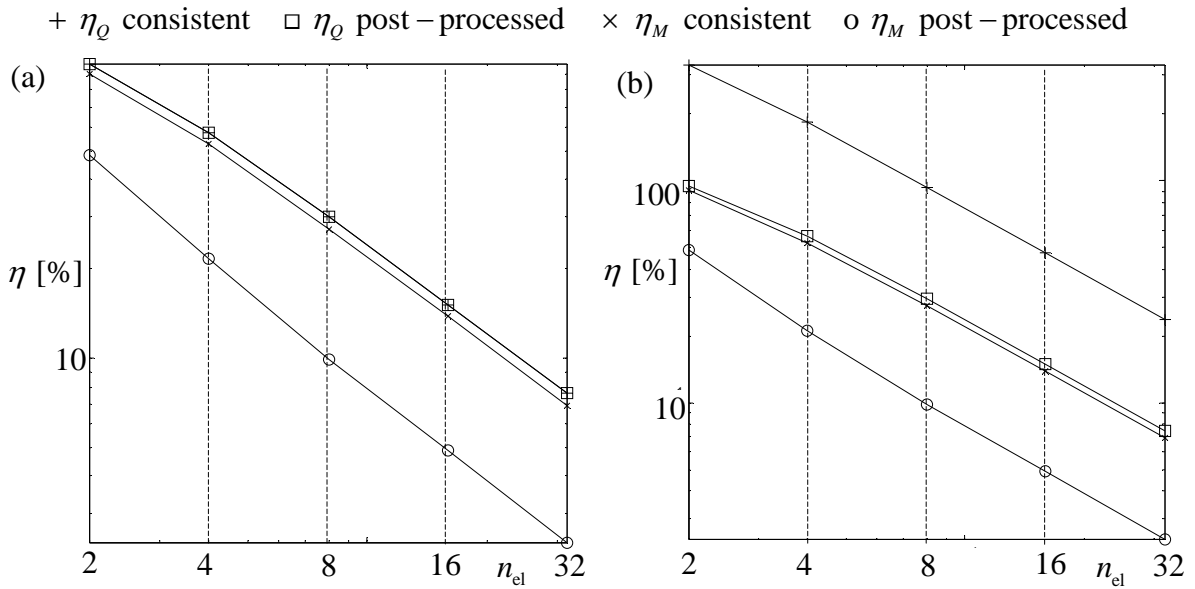


Figure B.1: Triangular elements, “hard” supports, nodal parameters from the analytical solution, distorted grid, (a) $\varepsilon = 10$ and (b) $\varepsilon = 0,01$

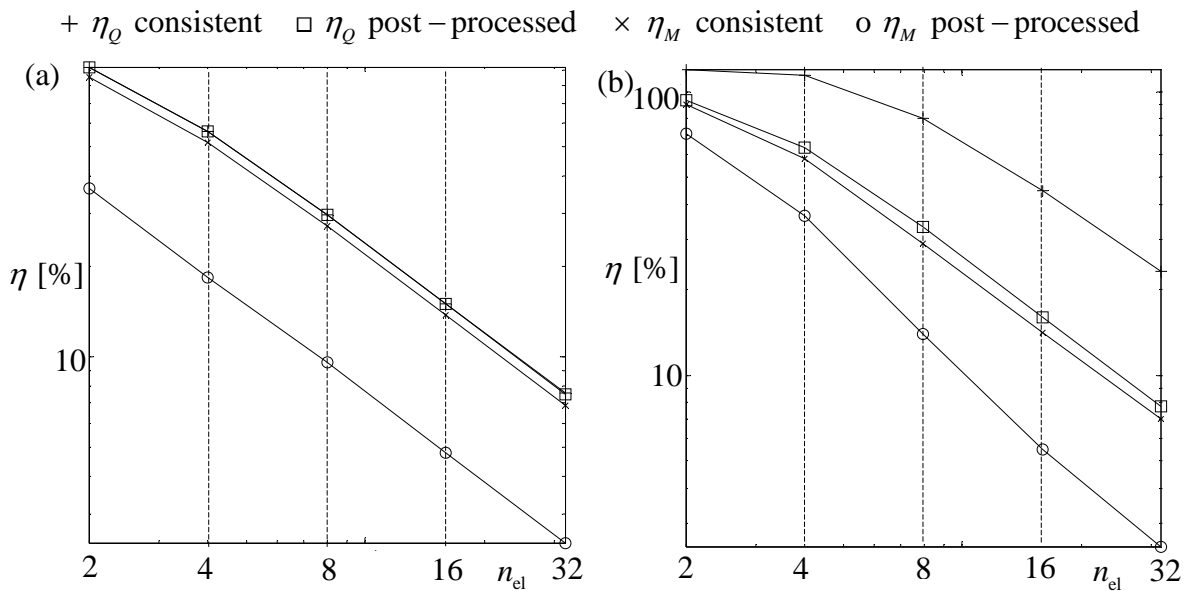


Figure B.2: Triangular elements, “hard” supports, nodal parameters from the finite element solution, distorted grid, (a) $\varepsilon = 10$ and (b) $\varepsilon = 0,01$

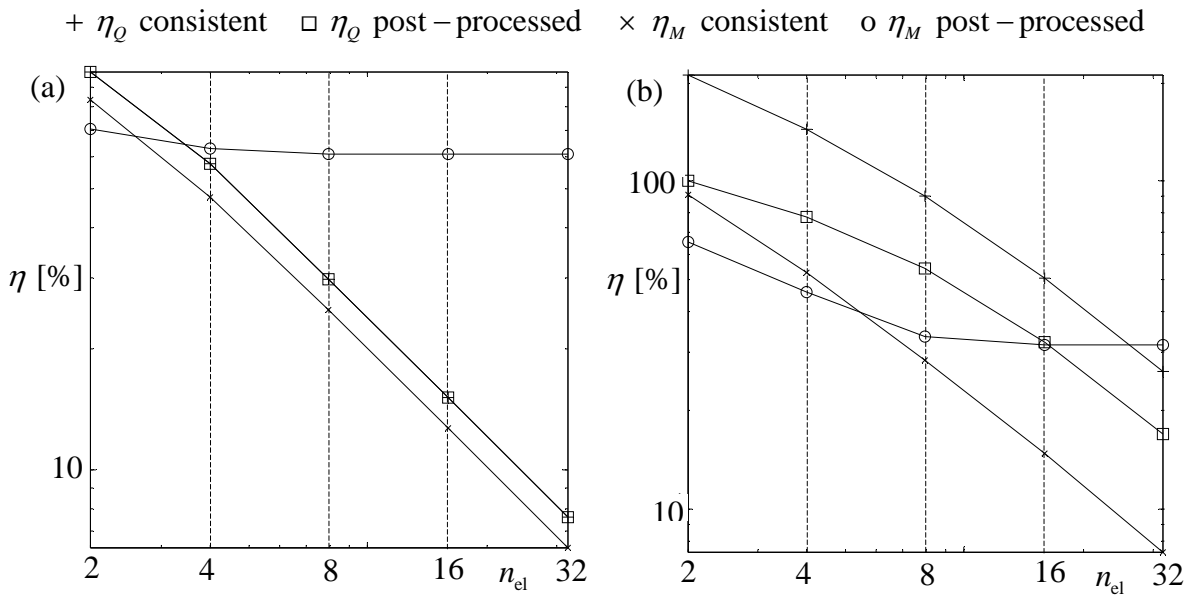


Figure B.3: Triangular elements, “mixed” supports, nodal parameters from the analytical solution, distorted grid, (a) $\varepsilon = 10$ and (b) $\varepsilon = 0,01$

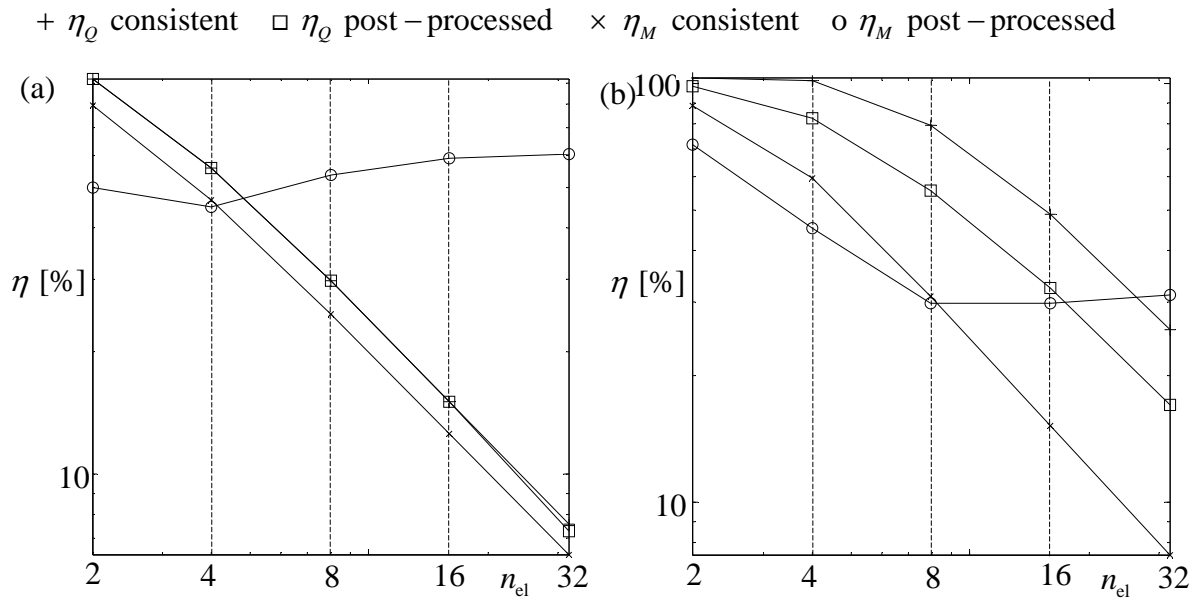


Figure B.4: Triangular elements, “mixed” supports, nodal parameters from the finite element solution, distorted grid, (a) $\varepsilon = 10$ and (b) $\varepsilon = 0,01$

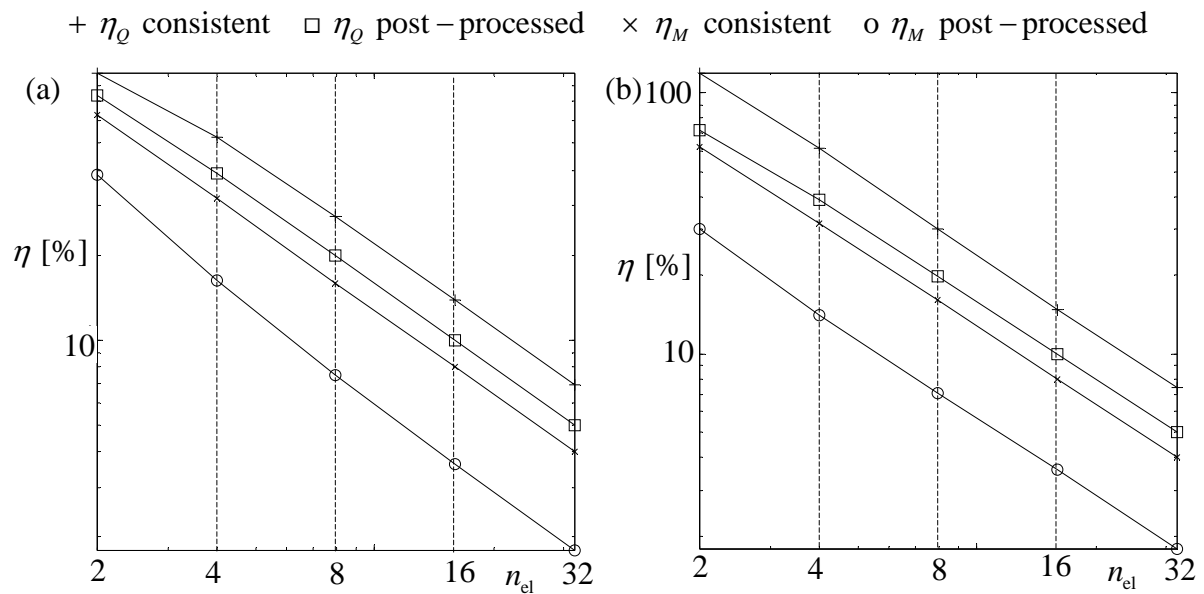


Figure B.5: Quadrilateral elements, “hard” supports, nodal parameters from the analytical solution, distorted grid, (a) $\varepsilon = 10$ and $\varepsilon = 0,01$

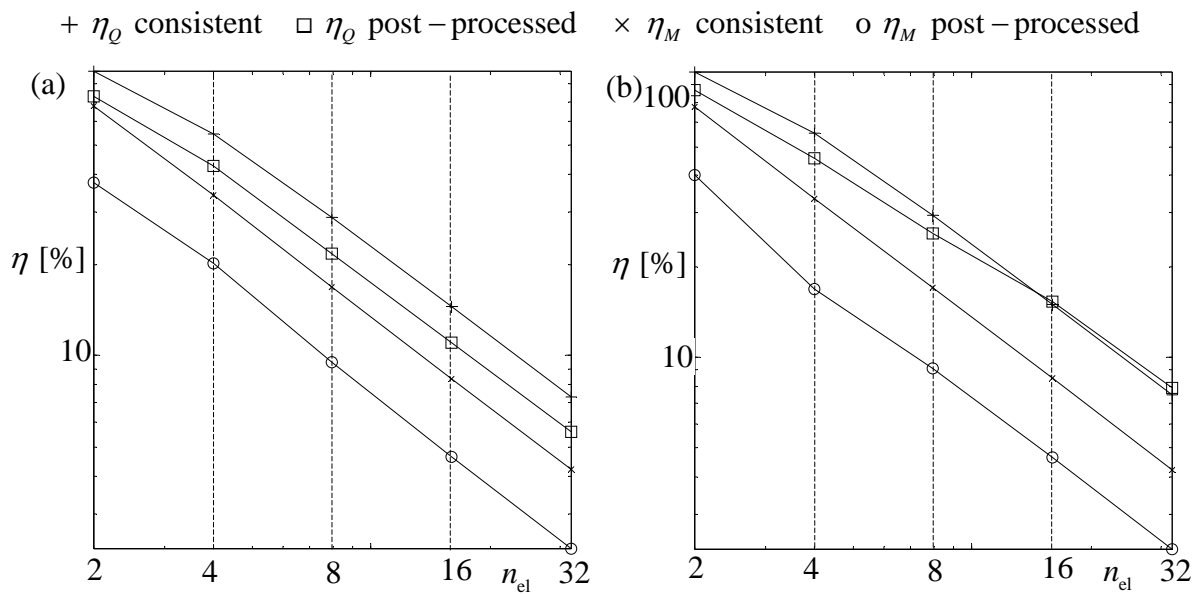


Figure B.6: Quadrilateral elements, “hard” supports, nodal parameters from the finite element solution, distorted grid, (a) $\varepsilon = 10$ and (b) $\varepsilon = 0,01$

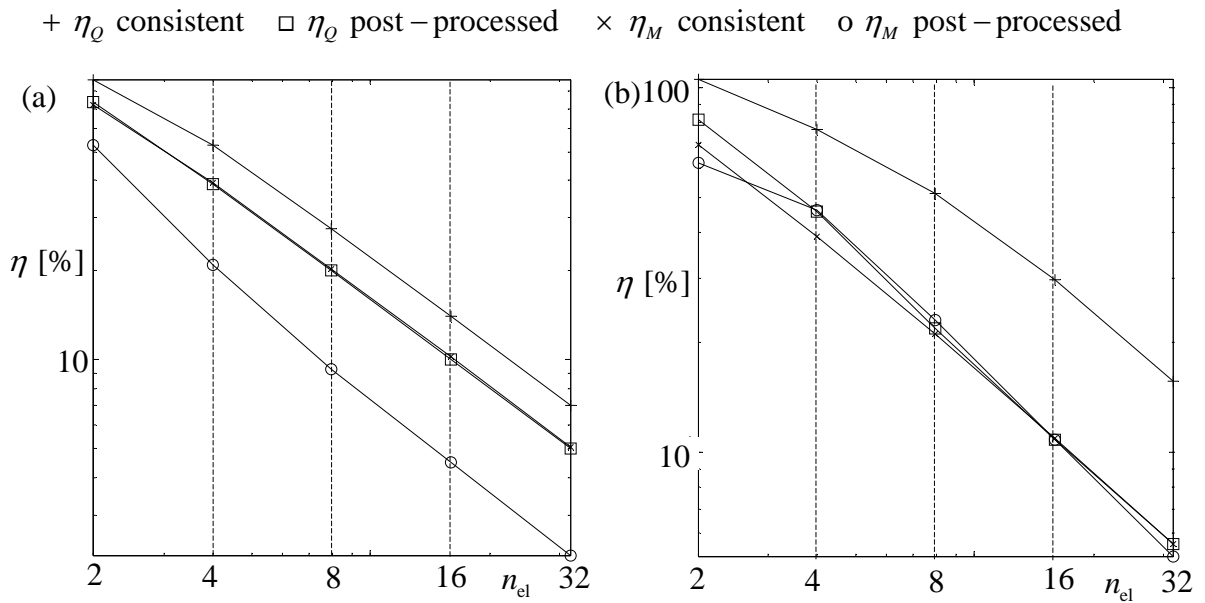


Figure B.7: Quadrilateral elements, “mixed” supports, nodal parameters from the analytical solution, distorted grid, (a) $\varepsilon = 10$ and (b) $\varepsilon = 0,01$

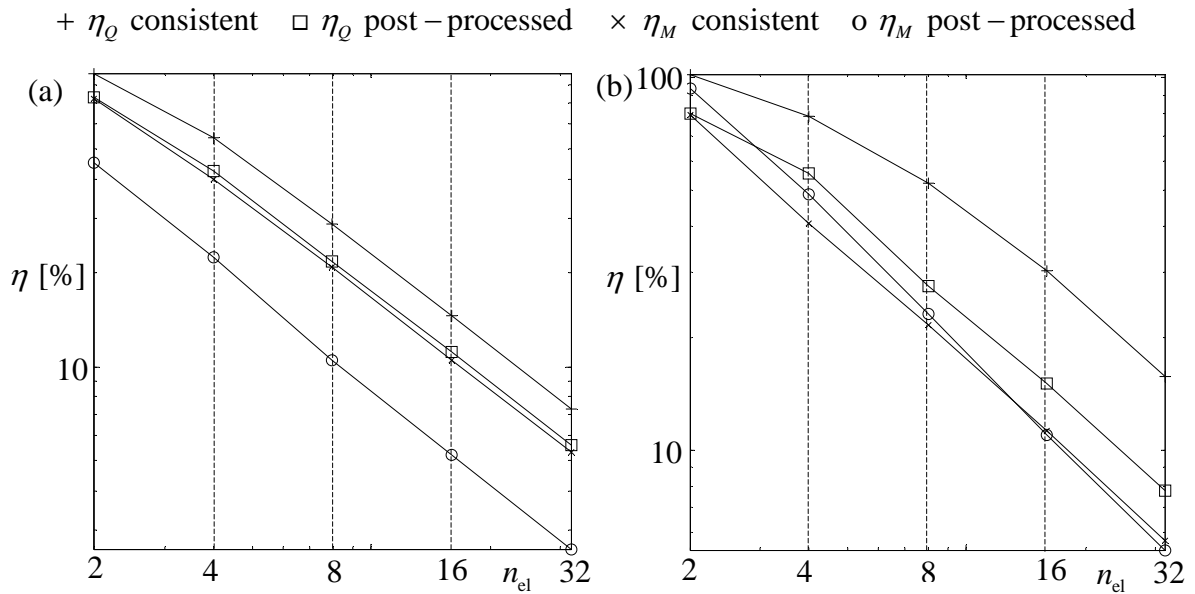


Figure B.8: Quadrilateral elements, “mixed” supports, nodal parameters from the finite element solution, distorted grid, (a) $\varepsilon = 10$ and (b) $\varepsilon = 0,01$

Appendix C: Constraint equation between the shear parameters \mathbf{b}^e

The shear parameters

$$\mathbf{b}_{n \times 1}^e = \left[\gamma_s^{12} \quad \dots \quad \gamma_s^{n1} \right]^T, \quad n = 3 \text{ or } 4 \quad (\text{C.1})$$

are not independent, but constrained by one compatibility equation. This equation is obtained as follows. Because the tangential shears of the element sides are assumed to be constants, the differences of the nodal deflections caused by shear corresponding to element side ij can be written as

$$w_j^s - w_i^s = \gamma_s^{ij} h_{ij}. \quad (\text{C.2})$$

Writing equations (C.2) for the sides of a triangular element gives

$$\begin{aligned} w_2^s - w_1^s &= \gamma_s^{12} h_{12}, \\ w_3^s - w_2^s &= \gamma_s^{23} h_{23}, \\ w_1^s - w_3^s &= \gamma_s^{31} h_{31}. \end{aligned} \quad (\text{C.3})$$

Summing these equations gives

$$\gamma_s^{12} h_{12} + \gamma_s^{23} h_{23} + \gamma_s^{31} h_{31} = 0. \quad (\text{C.4})$$

This equation is the shear compatibility equation of a triangular element. The corresponding equation for a quadrilateral element is obtained similarly and it is

$$\gamma_s^{12} h_{12} + \gamma_s^{23} h_{23} + \gamma_s^{34} h_{34} + \gamma_s^{41} h_{41} = 0. \quad (\text{C.5})$$

Appendix D: Why in a triangular element the three parameter shear approximation results to constant Cartesian shear components γ_x and γ_y within an element.

Multiplying the relations

$$\begin{aligned} \gamma_s^{ij} &= c_{ij} \gamma_{xj} + s_{ij} \gamma_{yj}, \\ \gamma_s^{jk} &= c_{jk} \gamma_{xj} + s_{jk} \gamma_{yj}, \end{aligned} \quad (\text{D.1})$$

which express the tangential shears γ_s^{ij} and γ_s^{jk} of the element sides connected to node j in terms of the Cartesian shears γ_{xj} and γ_{yj} of node j , respectively, by side lengths h_{ij} and h_{jk} and taking further into account the relations $x_{ij} \equiv x_j - x_i = c_{ij} h_{ij}$ and $y_{ij} \equiv y_j - y_i = s_{ij} h_{ij}$ gives

$$\begin{aligned}
x_{ji}\gamma_{xj} + y_{ji}\gamma_{yj} &= \gamma_s^{ij}h_{ij}, \\
x_{kj}\gamma_{xj} + y_{kj}\gamma_{yj} &= \gamma_s^{jk}h_{jk}.
\end{aligned}
\tag{D.2}$$

Solving the Cartesian shears from these equations gives

$$\begin{aligned}
\gamma_{xj} &= \frac{1}{2A}(y_{kj}\gamma_s^{ij}h_{ij} - y_{ji}\gamma_s^{jk}h_{jk}), \\
\gamma_{yj} &= \frac{1}{2A}(-x_{kj}\gamma_s^{ij}h_{ij} + x_{ji}\gamma_s^{jk}h_{jk}),
\end{aligned}
\tag{D.3}$$

where $A = (x_{ji}y_{kj} - y_{ji}x_{kj})/2$ is the area of the element. Similar expressions for the Cartesian shears of other nodes k and i are obtained using cyclic permutation. Subtracting the expressions of Cartesian shears of nodes i and j gives

$$\begin{aligned}
\gamma_{xi} - \gamma_{xj} &= \frac{y_{ji}}{2A}(\gamma_s^{12}h_{12} + \gamma_s^{23}h_{23} + \gamma_s^{31}h_{31}), \\
\gamma_{yi} - \gamma_{yj} &= -\frac{x_{ji}}{2A}(\gamma_s^{12}h_{12} + \gamma_s^{23}h_{23} + \gamma_s^{31}h_{31}).
\end{aligned}
\tag{D.4}$$

Based on the shear compatibility equation (C.4) of a triangular element, equations (D.4) now give $\gamma_{xi} = \gamma_{xj}$, $\gamma_{yi} = \gamma_{yj}$. Thus we conclude, that $\gamma_{x1} = \gamma_{x2} = \gamma_{x3}$ and $\gamma_{y1} = \gamma_{y2} = \gamma_{y3}$, and the Cartesian shear components γ_x and γ_y are constants within each element.